EUROPEAN ORGANIZATION FOR NUCLEAR RESEARCH

CERN–EP-PH/2005-029

30 June 2005

Study of double-tagged $\gamma\gamma$ events at LEPII

DELPHI Collaboration

Abstract

Double-tagged interactions of photons with virtualities Q^2 between 10 GeV^2 and 200 GeV^2 are studied with the data collected by DELPHI at LEPII from 1998 to 2000, corresponding to an integrated luminosity of 550 pb^{-1}. The $\gamma^*\gamma^* \to \mu^+\mu^-$ data agree with QED predictions. The cross-section of the reaction $\gamma^*\gamma^* \to hadrons$ is measured and compared to the LO and NLO BFKL calculations.

(Accepted by Euro. Phys. Journ. C)

J.Abdallah[25], P.Abreu[22], W.Adam[51], P.Adzic[11], T.Albrecht[17], T.Alderweireld[2], R.Alemany-Fernandez[8], T.Allmendinger[17], P.P.Allport[23], U.Amaldi[29], N.Amapane[45], S.Amato[48], E.Anashkin[36], A.Andreazza[28], S.Andringa[22], N.Anjos[22], P.Antilogus[25], W-D.Apel[17], Y.Arnoud[14], S.Ask[26], B.Asman[44], J.E.Augustin[25], A.Augustinus[8], P.Baillon[8], A.Ballestrero[46], P.Bambade[20], R.Barbier[27], D.Bardin[16], G.Barker[17], A.Baroncelli[39], M.Battaglia[8], M.Baubillier[25], K-H.Becks[53], M.Begalli[6], A.Behrmann[53], E.Ben-Haim[20], N.Benekos[32], A.Benvenuti[5], C.Berat[14], M.Berggren[25], L.Berntzon[44], D.Bertrand[2], M.Besancon[40], N.Besson[40], D.Bloch[9], M.Blom[31], M.Bluj[52], M.Bonesini[29], M.Boonekamp[40], P.S.L.Booth[23], G.Borisov[21], O.Botner[49], B.Bouquet[20], T.J.V.Bowcock[23], I.Boyko[16], M.Bracko[43], R.Brenner[49], E.Brodet[35], P.Bruckman[18], J.M.Brunet[7], L.Bugge[33], P.Buschmann[53], M.Calvi[29], T.Camporesi[8], V.Canale[38], F.Carena[8], N.Castro[22], F.Cavallo[5], M.Chapkin[42], Ph.Charpentier[8], P.Checchia[36], R.Chierici[8], P.Chliapnikov[42], J.Chudoba[8], S.U.Chung[8], K.Cieslik[18], P.Collins[8], R.Contri[13], G.Cosme[20], F.Cossutti[47], M.J.Costa[50], B.Crawley[1], D.Crennell[37], J.Cuevas[34], J.D'Hondt[2], J.Dalmau[44], T.da Silva[48], W.Da Silva[25], G.Della Ricca[47], A.De Angelis[47], W.De Boer[17], C.De Clercq[2], B.De Lotto[47], N.De Maria[45], A.De Min[36], L.de Paula[48], L.Di Ciaccio[38], A.Di Simone[39], K.Doroba[52], J.Drees[53,8], M.Dris[32], G.Eigen[4], T.Ekelof[49], M.Ellert[49], M.Elsing[8], M.C.Espirito Santo[22], G.Fanourakis[11], D.Fassouliotis[11,3], M.Feindt[17], J.Fernandez[41], A.Ferrer[50], F.Ferro[13], U.Flagmeyer[53], H.Foeth[8], E.Fokitis[32], F.Fulda-Quenzer[20], J.Fuster[50], M.Gandelman[48], C.Garcia[50], Ph.Gavillet[8], E.Gazis[32], R.Gokieli[8,52], B.Golob[43], G.Gomez-Ceballos[41], P.Goncalves[22], E.Graziani[39], G.Grosdidier[20], K.Grzelak[52], J.Guy[37], C.Haag[17], A.Hallgren[49], K.Hamacher[53], K.Hamilton[35], S.Haug[33], F.Hauler[17], V.Hedberg[26], M.Hennecke[17], H.Herr[8], J.Hoffman[52], S-O.Holmgren[44], P.J.Holt[8], M.A.Houlden[23], K.Hultqvist[44], J.N.Jackson[23], G.Jarlskog[26], P.Jarry[40], D.Jeans[35], E.K.Johansson[44], P.D.Johansson[44], P.Jonsson[27], C.Joram[8], L.Jungermann[17], F.Kapusta[25], S.Katsanevas[27], E.Katsoufis[32], G.Kernel[43], B.P.Kersevan[8,43], U.Kerzel[17], A.Kiiskinen[15], B.T.King[23], N.J.Kjaer[8], P.Kluit[31], P.Kokkinias[11], C.Kourkoumelis[3], O.Kouznetsov[16], Z.Krumstein[16], M.Kucharczyk[18], J.Lamsa[1], G.Leder[51], F.Ledroit[14], L.Leinonen[44], R.Leitner[30], J.Lemonne[2], V.Lepeltier[20], T.Lesiak[18], W.Liebig[53], D.Liko[51], A.Lipniacka[44], J.H.Lopes[48], J.M.Lopez[34], D.Loukas[11], P.Lutz[40], L.Lyons[35], J.MacNaughton[51], A.Malek[53], S.Maltezos[32], F.Mandl[51], J.Marco[41], R.Marco[41], B.Marechal[48], M.Margoni[36], J-C.Marin[8], C.Mariotti[8], A.Markou[11], C.Martinez-Rivero[41], J.Masik[12], N.Mastroyiannopoulos[11], F.Matorras[41], C.Matteuzzi[29], F.Mazzucato[36], M.Mazzucato[36], R.Mc Nulty[23], C.Meroni[28], W.T.Meyer[1], E.Migliore[45], W.Mitaroff[51], U.Mjoernmark[26], T.Moa[44], M.Moch[17], K.Moenig[8,10], R.Monge[13], J.Montenegro[31], D.Moraes[48], S.Moreno[22], P.Morettini[13], U.Mueller[53], K.Muenich[53], M.Mulders[31], L.Mundim[6], W.Murray[37], B.Muryn[19], G.Myatt[35], T.Myklebust[33], M.Nassiakou[11], F.Navarria[5], K.Nawrocki[52], R.Nicolaidou[40], M.Nikolenko[16,9], A.Oblakowska-Mucha[19], V.Obraztsov[42], A.Olshevski[16], A.Onofre[22], R.Orava[15], K.Osterberg[15], A.Ouraou[40], A.Oyanguren[50], M.Paganoni[29], S.Paiano[5], J.P.Palacios[23], H.Palka[18], Th.D.Papadopoulou[32], L.Pape[8], C.Parkes[24], F.Parodi[13], U.Parzefall[8], A.Passeri[39], O.Passon[53], L.Peralta[22], V.Perepelitsa[50], A.Perrotta[5], A.Petrolini[13], J.Piedra[41], L.Pieri[39], F.Pierre[40], M.Pimenta[22], E.Piotto[8], T.Podobnik[43], V.Poireau[8], M.E.Pol[6], G.Polok[18], P.Poropat[†47], V.Pozdniakov[16], N.Pukhaeva[2,16], A.Pullia[29], J.Rames[12], L.Ramler[17], A.Read[33], P.Rebecchi[8], J.Rehn[17], D.Reid[31], R.Reinhardt[53], P.Renton[35], F.Richard[20], J.Ridky[12], M.Rivero[41], D.Rodriguez[41], A.Romero[45], P.Ronchese[36], E.Rosenberg[1], P.Roudeau[20], T.Rovelli[5], V.Ruhlmann-Kleider[40], D.Ryabtchikov[42], A.Sadovsky[16], L.Salmi[15], J.Salt[50], A.Savoy-Navarro[25], U.Schwickerath[8], A.Segar[35], R.Sekulin[37], M.Siebel[53], A.Sisakian[16], G.Smadja[27], O.Smirnova[26], A.Sokolov[42], A.Sopczak[21], R.Sosnowski[52], T.Spassov[8], M.Stanitzki[17], A.Stocchi[20], J.Strauss[51], B.Stugu[4], M.Szczekowski[52], M.Szeptycka[52], T.Szumlak[19], T.Tabarelli[29], A.C.Taffard[23], F.Tegenfeldt[49], J.Timmermans[31], L.Tkatchev[16], M.Tobin[23], S.Todorovova[12], B.Tome[22], A.Tonazzo[29], P.Tortosa[50], P.Travnicek[12], D.Treille[8], G.Tristram[7], M.Trochimczuk[52], C.Troncon[28], M-L.Turluer[40], P.Tyapkin[16], S.Tzamarias[11], V.Uvarov[42], G.Valenti[5], P.Van Dam[31], J.Van Eldik[8], A.Van Lysebetten[2], N.van Remortel[2], I.Van Vulpen[8], G.Vegni[28], F.Veloso[22], W.Venus[37], P.Verdier[27], Yu.L.Vertogradova[16], V.Verzi[38], D.Vilanova[40], L.Vitale[47], V.Vrba[12], H.Wahlen[53], A.J.Washbrook[23], C.Weiser[17],

D.Wicke[8], J.Wickens[2], G.Wilkinson[35], M.Winter[9], M.Witek[18], O.Yushchenko[42], A.Zalewska[18], P.Zalewski[52], D.Zavrtanik[43], V.Zhuravlov[16], N.I.Zimin[16], A.Zintchenko[16], M.Zupan[11]

[1]Department of Physics and Astronomy, Iowa State University, Ames IA 50011-3160, USA
[2]Physics Department, Universiteit Antwerpen, Universiteitsplein 1, B-2610 Antwerpen, Belgium
and IIHE, ULB-VUB, Pleinlaan 2, B-1050 Brussels, Belgium
and Faculté des Sciences, Univ. de l'Etat Mons, Av. Maistriau 19, B-7000 Mons, Belgium
[3]Physics Laboratory, University of Athens, Solonos Str. 104, GR-10680 Athens, Greece
[4]Department of Physics, University of Bergen, Allégaten 55, NO-5007 Bergen, Norway
[5]Dipartimento di Fisica, Università di Bologna and INFN, Via Irnerio 46, IT-40126 Bologna, Italy
[6]Centro Brasileiro de Pesquisas Físicas, rua Xavier Sigaud 150, BR-22290 Rio de Janeiro, Brazil
and Depto. de Física, Pont. Univ. Católica, C.P. 38071 BR-22453 Rio de Janeiro, Brazil
and Inst. de Física, Univ. Estadual do Rio de Janeiro, rua São Francisco Xavier 524, Rio de Janeiro, Brazil
[7]Collège de France, Lab. de Physique Corpusculaire, IN2P3-CNRS, FR-75231 Paris Cedex 05, France
[8]CERN, CH-1211 Geneva 23, Switzerland
[9]Institut de Recherches Subatomiques, IN2P3 - CNRS/ULP - BP20, FR-67037 Strasbourg Cedex, France
[10]Now at DESY-Zeuthen, Platanenallee 6, D-15735 Zeuthen, Germany
[11]Institute of Nuclear Physics, N.C.S.R. Demokritos, P.O. Box 60228, GR-15310 Athens, Greece
[12]FZU, Inst. of Phys. of the C.A.S. High Energy Physics Division, Na Slovance 2, CZ-180 40, Praha 8, Czech Republic
[13]Dipartimento di Fisica, Università di Genova and INFN, Via Dodecaneso 33, IT-16146 Genova, Italy
[14]Institut des Sciences Nucléaires, IN2P3-CNRS, Université de Grenoble 1, FR-38026 Grenoble Cedex, France
[15]Helsinki Institute of Physics and Department of Physical Sciences, P.O. Box 64, FIN-00014 University of Helsinki, Finland
[16]Joint Institute for Nuclear Research, Dubna, Head Post Office, P.O. Box 79, RU-101 000 Moscow, Russian Federation
[17]Institut für Experimentelle Kernphysik, Universität Karlsruhe, Postfach 6980, DE-76128 Karlsruhe, Germany
[18]Institute of Nuclear Physics PAN,Ul. Radzikowskiego 152, PL-31142 Krakow, Poland
[19]Faculty of Physics and Nuclear Techniques, University of Mining and Metallurgy, PL-30055 Krakow, Poland
[20]Université de Paris-Sud, Lab. de l'Accélérateur Linéaire, IN2P3-CNRS, Bât. 200, FR-91405 Orsay Cedex, France
[21]School of Physics and Chemistry, University of Lancaster, Lancaster LA1 4YB, UK
[22]LIP, IST, FCUL - Av. Elias Garcia, 14-1^o, PT-1000 Lisboa Codex, Portugal
[23]Department of Physics, University of Liverpool, P.O. Box 147, Liverpool L69 3BX, UK
[24]Dept. of Physics and Astronomy, Kelvin Building, University of Glasgow, Glasgow G12 8QQ
[25]LPNHE, IN2P3-CNRS, Univ. Paris VI et VII, Tour 33 (RdC), 4 place Jussieu, FR-75252 Paris Cedex 05, France
[26]Department of Physics, University of Lund, Sölvegatan 14, SE-223 63 Lund, Sweden
[27]Université Claude Bernard de Lyon, IPNL, IN2P3-CNRS, FR-69622 Villeurbanne Cedex, France
[28]Dipartimento di Fisica, Università di Milano and INFN-MILANO, Via Celoria 16, IT-20133 Milan, Italy
[29]Dipartimento di Fisica, Univ. di Milano-Bicocca and INFN-MILANO, Piazza della Scienza 2, IT-20126 Milan, Italy
[30]IPNP of MFF, Charles Univ., Areal MFF, V Holesovickach 2, CZ-180 00, Praha 8, Czech Republic
[31]NIKHEF, Postbus 41882, NL-1009 DB Amsterdam, The Netherlands
[32]National Technical University, Physics Department, Zografou Campus, GR-15773 Athens, Greece
[33]Physics Department, University of Oslo, Blindern, NO-0316 Oslo, Norway
[34]Dpto. Fisica, Univ. Oviedo, Avda. Calvo Sotelo s/n, ES-33007 Oviedo, Spain
[35]Department of Physics, University of Oxford, Keble Road, Oxford OX1 3RH, UK
[36]Dipartimento di Fisica, Università di Padova and INFN, Via Marzolo 8, IT-35131 Padua, Italy
[37]Rutherford Appleton Laboratory, Chilton, Didcot OX11 OQX, UK
[38]Dipartimento di Fisica, Università di Roma II and INFN, Tor Vergata, IT-00173 Rome, Italy
[39]Dipartimento di Fisica, Università di Roma III and INFN, Via della Vasca Navale 84, IT-00146 Rome, Italy
[40]DAPNIA/Service de Physique des Particules, CEA-Saclay, FR-91191 Gif-sur-Yvette Cedex, France
[41]Instituto de Fisica de Cantabria (CSIC-UC), Avda. los Castros s/n, ES-39006 Santander, Spain
[42]Inst. for High Energy Physics, Serpukov P.O. Box 35, Protvino, (Moscow Region), Russian Federation
[43]J. Stefan Institute, Jamova 39, SI-1000 Ljubljana, Slovenia and Laboratory for Astroparticle Physics,
Nova Gorica Polytechnic, Kostanjeviska 16a, SI-5000 Nova Gorica, Slovenia,
and Department of Physics, University of Ljubljana, SI-1000 Ljubljana, Slovenia
[44]Fysikum, Stockholm University, Box 6730, SE-113 85 Stockholm, Sweden
[45]Dipartimento di Fisica Sperimentale, Università di Torino and INFN, Via P. Giuria 1, IT-10125 Turin, Italy
[46]INFN,Sezione di Torino and Dipartimento di Fisica Teorica, Università di Torino, Via Giuria 1, IT-10125 Turin, Italy
[47]Dipartimento di Fisica, Università di Trieste and INFN, Via A. Valerio 2, IT-34127 Trieste, Italy
and Istituto di Fisica, Università di Udine, IT-33100 Udine, Italy
[48]Univ. Federal do Rio de Janeiro, C.P. 68528 Cidade Univ., Ilha do Fundão BR-21945-970 Rio de Janeiro, Brazil
[49]Department of Radiation Sciences, University of Uppsala, P.O. Box 535, SE-751 21 Uppsala, Sweden
[50]IFIC, Valencia-CSIC, and D.F.A.M.N., U. de Valencia, Avda. Dr. Moliner 50, ES-46100 Burjassot (Valencia), Spain
[51]Institut für Hochenergiephysik, Österr. Akad. d. Wissensch., Nikolsdorfergasse 18, AT-1050 Vienna, Austria
[52]Inst. Nuclear Studies and University of Warsaw, Ul. Hoza 69, PL-00681 Warsaw, Poland
[53]Fachbereich Physik, University of Wuppertal, Postfach 100 127, DE-42097 Wuppertal, Germany
† deceased

1 Introduction

This paper presents the study of double-tagged two-photon interactions $e^+e^- \rightarrow e^+e^-\gamma^*\gamma^* \rightarrow e^+e^-X$ (where X is either a muon pair or hadrons) with the DELPHI detector [1] at the CERN LEPII collider. Both scattered electrons[1] are detected by the Small angle TIle Calorimeter (STIC). Compared to the untagged or single-tagged modes, with both or one of the electrons escaping detection, this mode of gamma-gamma collision has the advantage that the kinematics of the interaction is well defined by the measurement of the energies and scattering angles of the tagged particles. The production of muon pairs is described by QED. Similarly, multihadron production is expected to be described by QPM, but only in a first approximation. If the virtualities of the photons are large enough, it is predicted that there should be a large contribution from processes with (multi)gluon exchange between $q\bar{q}$ dipoles [2], which is described by the BFKL equation [3]. Two-photon interactions are therefore a suitable process to investigate BFKL dynamics. Figure 1 shows the main diagrams relevant to the analysis.

The kinematics of the process is illustrated in Figure 2. We use the following notations: p_i (i=1,2) are the four-momenta of the beam electrons, $\sqrt{s}$ is the e^+e^- centre-of-mass energy, E_{beam} is the beam energy; the four-momenta of the scattered electrons, their polar angles and their energies are $p_i^{'}$, θ_i and E_i respectively.

The variables relevant to this study are the virtualities of the photons, Q_i^2, the invariant mass of the two photons $W_{\gamma^*\gamma^*}$ and a dimensionless variable Y:

- $Q_i^2 = -q_i^2 = -(p_i - p_i^{'})^2 = 4E_iE_{beam}\sin^2(\theta_i/2)$;
- $W_{\gamma^*\gamma^*}^2 = -(q_1+q_2)^2 \simeq sy_1y_2$ with $y_i = 1-(E_i/E_{beam})\cos^2(\theta_i/2)$;
- $Y = \ln(W_{\gamma^*\gamma^*}^2/\sqrt{Q_1^2Q_2^2})$.

The Y variable is used to compare the multihadron data with the BFKL predicted cross-section with the conditions $W_{\gamma^*\gamma^*}^2 \gg Q_i^2$ and $\mid \ln(Q_1^2/Q_2^2) \mid < 1$, where the second condition is needed to select virtualities of the photons of the same order.

The analysis is divided into two parts: the study of the production of muon pairs aims at comparing the data with the well-known QED model and at tuning the experimental cuts, while the multihadron production is used to measure the cross-section $\sigma_{\gamma^*\gamma^*}$ and to compare it with the BFKL predictions. The models used for each part and the background estimations are described separately.

2 Detector and data sample

A detailed description of the DELPHI detector and of its performance is presented in ref. [1]: here only the components relevant to the present analysis will be briefly mentioned.

The scattered electrons are detected in the luminosity monitor STIC, which covers the region from 29 mrad to 185 mrad in the polar angle θ [2], with $R\phi$ segmentation of 3 cm $\times 22.5^\circ$ [4]. Given the energy and angular resolution of the STIC calorimeter, the Q^2

[1] Throughout this paper, electron stands both for electron and positron. Asterisk over γ symbol explicitly indicates that the photon is highly virtual.

[2] The origin of the DELPHI reference system was at the centre of the detector. It coincides with the ideal interaction point. The z-axis was parallel to the e^- beam, the x-axis pointed horizontally to the centre of the LEP ring and the y-axis was vertically upward. The co-ordinates R, ϕ,z formed a cylindrical coordinate system and θ was the polar angle with respect to the z-axis.

resolution varies between 1 GeV^2 and 2.5 GeV^2 in the Q^2 domain of the present analysis (Q_i^2 between 10 GeV^2 and 200 GeV^2).

Charged particles are detected in the barrel tracking system comprising the Silicon Tracker (ST), the Inner Detector (ID), the Time Projection Chamber (TPC), and the Outer Detector. In the endcap regions, they are detected by the ST, by the TPC down to 20° in polar angle, by the ID down to 15° and by the Forward Chambers A and B. All detectors are located inside a superconducting solenoid providing a uniform magnetic field of 1.23 T parallel to the axis of the colliding e^+e^- beams. The combined momentum resolution provided by the tracking system is a few per-mille in the momentum range of this study.

Muon tagging is performed with the Barrel and the Forward muon drift chambers, and with the Surround Muon Chambers based on limited streamer tubes, which cover the gap between the previous two.

The study is done with the DELPHI data taken during 1998-2000 at e^+e^- centre-of-mass energies from 189 GeV to 209 GeV, corresponding to an integrated luminosity of 550 pb^{-1}, with the subdetectors relevant for the analysis all fully operational.

Simulated events for the physics processes and backgrounds are generated at the different centre-of-mass energies and passed through the full DELPHI simulation and reconstruction chain.

3 Study of $e^+e^- \to e^+e^- + \mu^+\mu^-$ interactions

3.1 Data analysis

The following criteria are used to select $\gamma^*\gamma^* \to \mu^+\mu^-$ events:

- There are two clusters with energy deposition E_i greater than 30 GeV, one in each arm of the STIC [3], and the polar angle θ_i (or (180°-θ_i) if the angle is more than 90°) exceeds 2.2° for each cluster;
- Q_i^2 is between 10 GeV^2 and 200 GeV^2 for both tagged particles;
- The acollinearity of the scattered electrons is above 0.2 degrees. This criterion removes a superposition between Bhabha events and untagged $\gamma\gamma \to \mu^+\mu^-$ events;
- Each event contains two charged particles with zero net charge and invariant mass between 2 GeV/c^2 and 50 GeV/c^2. Particles are considered if their momentum is greater than 400 MeV/c, their polar angle is within the interval 20° - 160° and their impact parameters are smaller than 4 cm in $R\phi$ and 10 cm in z;
- At least one of the charged particles is identified as a 'standard' or 'tight' muon by the DELPHI tagging algorithm [1].

The number of selected $e^+e^- \to e^+e^- + \mu^+\mu^-$ events is 226. Double-tagged events are triggered either by the STIC trigger component or by a single charged particle track component [5]. The trigger efficiency has been calculated using the redundancy of the trigger together with independent calculations based on the parameterization of the single track efficiency [5], and is found to be larger than 99%.

The BDKRC event generator [6], including the full set of QED diagrams and all fermion masses, is used for the Monte Carlo simulation of $\gamma^*\gamma^* \to \mu^+\mu^-$ events. The processes corresponding to diagrams other than the diagram of two-photon interactions

[3] The choice of the cutoff for the minimum energy of the tagged particles has to be made carefully. It should be as small as possible since low electron energy corresponds to large values of $W_{\gamma^*\gamma^*}$ and Y (which are important in the multihadron case, see below). At the same time the lowering of this cut leads to an increase of the off-momentum background and thus decreases the accuracy of the measurement.

(multiperipheral) are found to give a contribution of about 2 percent. The number of multiperipheral events is expected to be 194.

The following sources of background are considered:

- The coincidence of a gamma-gamma event with an off-momentum electron. The probability of such coincidences, averaged over the data from different years, is calculated with $\gamma\gamma \to \mu^+\mu^-$ events to be (0.0016 ± 0.0002). Using this value, the background from a superimposition of two off-momentum electrons with an untagged $\gamma\gamma \to \mu^+\mu^-$ event turns out to be negligible;
- The coincidence of one off-momentum electron with a $\gamma^*\gamma \to \mu^+\mu^-$ single-tagged event, i.e. when one scattered electron is detected in the STIC while the other one is an off-momentum electron. Usually this background is evaluated by convoluting the $\gamma^*\gamma \to \mu^+\mu^-$ Monte Carlo simulation with the spectrum of off-momentum electrons. This requires the appropriate description of the single-tagged data by the simulation and thus it is model-dependent. The following approach avoids the problem and calculates the background directly from the data. The cuts as listed above are applied with one difference: events with two electrons in the same STIC arm and none in the other are selected. They include one off-momentum electron. Then one of the electrons is rotated to the "empty" STIC arm, i.e. its p_z component is inverted. The background coming from the coincidence of one off-momentum with a $\gamma^*\gamma \to \mu^+\mu^-$ single-tagged event is thus estimated to be (15 ± 4) events;
- The background from $\gamma^*\gamma^* \to \tau^+\tau^-$ events is estimated as (23 ± 2) events by using the TWOGAM event generator [7].

The overall background is thus estimated as (38 ± 4) events.

Figure 3 shows the distributions of the tagged particle energies[4] normalized to the beam energy, their polar angles (two entries per event for both histograms), the invariant mass of the muon pair, $W_{\mu\mu}$, calculated from the muon 4-momenta, and the distribution of the normalized longitudinal momentum balance defined as

$$NLMB = \mid p_{z,tag1} + p_{z,tag2} + p_{z,X} \mid / E_{beam},$$

where $p_{z,X}$ is the $z-$component of the momentum of the system produced in the $\gamma^*\gamma^*$ collision. This variable has to be peaked at zero for well-reconstructed events and it is sensitive to the final state radiation.

The analysis of $\gamma^*\gamma^* \to \mu^+\mu^-$ events permits the quality of the reconstruction to be examined. The kinematics of the gamma-gamma system is completely determined by the measurements of the muons and of the tagged electrons in this exclusive channel, and some quantities can be calculated either from the tagged particles or from the muons. Figure 4a (b) shows the difference between the gamma-gamma invariant mass (Y variable) calculated from the muon 4-momenta $W_{\mu\mu}(Y_{\mu\mu})$ and that reconstructed from the tagged particles' measurements $W_{\gamma^*\gamma^*}(Y_{\gamma\gamma})$. The asymmetry of the distributions is due to radiative corrections, as it has been verified by Monte Carlo simulation. These comparisons show that the use of tagged particles is a good approximation to calculate the kinematic variables of the gamma-gamma system.

3.2 Results

The selected data sample is used for the measurement of the cross-section (σ_{ee}) of the reaction $e^+e^- \to e^+e^- + \mu^+\mu^-$. The corrections for the detector acceptance and efficiency are done with the BDKRC simulated events. The statistical uncertainty in the

[4] If the measured value of the electron energy is greater than E_{beam}, it is changed to (E_{beam}-0.5 GeV) to be able to calculate the $\gamma^*\gamma^*$ invariant mass.

MC simulation is included in the systematic error. Additional systematic uncertainties are evaluated by varying the selection criteria on the tagging particles. Systematic uncertainty coming from the muon identification procedure is negligible (second item of [1], p.96 and references therein).

The measured total σ_{ee} cross-section is $(1.38 \pm 0.12(stat) \pm 0.06(syst))$ pb for virtualities of the interacting photons, Q_i^2, between 10 GeV^2 and 200 GeV^2 and for invariant mass $W_{\mu\mu}$ between 2 GeV/c^2 and 50 GeV/c^2. The QED expectation, including radiative corrections, is (1.36 ± 0.01) pb. The cross-section calculated without radiative corrections is about 8% lower.

The σ_{ee} cross-section can be expressed via the flux of photons with different polarization and the corresponding partial cross-sections of the $\gamma^*\gamma^* \to \mu^+\mu^-$ interaction. This extraction procedure is described in the next section for multihadron production. Here only the result for the differential $\gamma^*\gamma^* \to \mu^+\mu^-$ cross-section as a function of Y is shown in figure 5. There is good agreement between the measurements and the QED predictions.

4 Study of $e^+e^- \to e^+e^- + hadrons$ interactions

4.1 Data analysis

The selection criteria for tagging electrons and for the charged particles are the same as described in the previous section. The sample of $\gamma^*\gamma^* \to hadrons$ events is then selected by the following criterion:

- Each event contains at least 3 charged particles with the invariant mass calculated from the particles' 4-momenta, W_{had}, larger than 2 GeV/c^2;

The following additional cuts are applied to suppress background events:

- If the energy of one cluster in STIC, normalized to the beam energy, is larger than 0.85 then the energy of another cluster has to be below 0.5. This cut is intended to suppress the contamination coming from $e^+e^- \to hadrons$ events;
- The thrust value of the charged particles, calculated in their centre-of-mass system, is less than 0.98 for the events with charged multiplicity below 5. The cut removes most of the $\gamma^*\gamma^* \to \tau^+\tau^-$ events.

After these requirements, 434 events have been selected. Again the trigger efficiency [5] can be estimated from the redundancy of the trigger and from a parameterization of the single track efficiency, and is larger than 99%.

The event generators used to simulate the $\gamma^*\gamma^*$ events and the background processes are listed below as well as the respective expected contributions:

- TWOGAM (version 2.02) [7] and PYTHIA (version 6.205) [8] event generators (both include radiative corrections) are used to simulate $\gamma^*\gamma^*$ interactions. The expectations are (331 ± 8) and (330 ± 8) events, respectively. The Monte Carlo generators include the quark-parton model (QPM) part and also the leading-order predictions for the resolved photon contribution;
- The background coming from the process $e^+e^- \to hadrons$ is simulated with the KK2f generator (version 4.14) [9] and its contribution is estimated to be (27 ± 3) events;
- The background of τ pairs produced in e^+e^- annihilation is found to be negligible;

- The contamination of τ pairs produced in the two-photon interactions is evaluated as (26 ± 3) events by using the TWOGAM program;
- The coincidence of an off-momentum electron with a $\gamma^*\gamma \to hadrons$ single-tagged event is evaluated as (5 ± 2) events by using the same approach as described in the previous section.

The data distributions for the photon virtualities, Q_i^2 (two entries per event), the invariant mass of the hadron system calculated with the charged particles' 4-momenta, W_{had}, the charged particles' multiplicity and the Y variable calculated with $W_{\gamma^*\gamma^*}$ are compared with the Monte Carlo simulation in figure 6. The data are represented with error bars. The solid and dashed histograms correspond to the sum of $\gamma^*\gamma^*$ simulated events obtained with the PYTHIA and TWOGAM generators, respectively, and various background sources. The hatched histograms show the estimated background contamination. Both $\gamma^*\gamma^*$ models agree reasonably well with the data. The excess of the data over Monte Carlo (for low Q^2, large W) already indicates that the QPM term is insufficient.

The calculations of the detector acceptance and efficiency have been done for both $\gamma^*\gamma^*$ models and are shown in figure 7. The detection efficiencies express slightly different behaviour - the TWOGAM values are larger than the PYTHIA ones for high values of the Y variable, while for small Y values the behaviour is the opposite. The decrease of the efficiencies for Y above 4 is due to the selection criteria.

4.2 Results

The background subtracted data are corrected for detector effects using the two models, and the measured differential cross-sections $d\sigma_{ee}/dY$ are shown in figure 8 together with the average expectation of the two event generators used. The uncertainty due to the migration of events caused by the finite Q^2 resolution (the relative uncertainty is around 0.08) is found to be small in comparison with the statistical uncertainty of the measurement. Note that, irrespective of the model, the data indicate a somewhat larger cross-section compared to expectations for high values of Y corresponding to large invariant masses of the $\gamma\gamma$ system. The total cross-section σ_{ee} of the $e^+e^- \to e^+e^- + hadrons$ interactions, within the phase space limited by the criteria Q_i^2 between 10 GeV^2 and 200 GeV^2, and W_{had} above 2 GeV/c^2, is measured to be (2.09 ± 0.17) pb using the corrections for detector effects based on TWOGAM and (1.86 ± 0.14) pb for the corrections based on PYTHIA. The statistical and systematic (see later) uncertainties are added in quadrature. The expectation of the quark-parton model is (1.81 ± 0.02) pb as obtained with TWOGAM.

The $\gamma^*\gamma^* \to hadrons$ interactions are expected to be sensitive to multiple gluon exchange (fig.1). The multigluon ladder is described by the BFKL equation [3], which predicts a growth of the cross-section at large Y. Note that the BFKL calculations are valid provided $W^2_{\gamma^*\gamma^*} \gg Q_i^2$ (the variable Y should be larger than 2) and $|\ln(Q_1^2/Q_2^2)| < 1$ (to maintain the photon virtualities approximately equal). The application of this latter condition has the effect of reducing the data sample by about 37%. It has to be mentioned however that the migration of events around the chosen cut at unity does not introduce an appreciable systematic uncertainty. According to the Monte Carlo simulation, around 3% of the selected sample had the true value of the logarithm above unity and pass the cut due to the Q^2 resolution. Approximately the same percentage migrates inversely.

The experimental conditions of the present study ($Q_i^2 \gg m_e^2$ and the symmetry requirement for tagged particle detection) permit the relation between σ_{ee} and $\sigma_{\gamma^*\gamma^*}$, which initially reads [10] (the interference terms are omitted):

$$\sigma_{ee} = \sum_{i,j=T,L} L_{ij}\sigma_{ij},$$

to be simplified to a relation involving an effective cross-section $\sigma_{\gamma^*\gamma^*}$,

$$\sigma_{ee} = L_{TT}\sigma_{\gamma^*\gamma^*} \text{ with } \sigma_{\gamma^*\gamma^*} = \sigma_{TT} + 2\epsilon\sigma_{LT} + \epsilon^2\sigma_{LL},$$

where L_{TT} is the flux of the transversely polarized photons calculable in QED, ϵ is around 0.94, $\sigma_{LT} \simeq 0.2\sigma_{TT}$ and $\sigma_{LL} \simeq 0.05\sigma_{TT}$ [11]. The TWOGAM event generator including QED radiative corrections has been used to calculate L_{TT}: it uses the decomposition of the cross-section for different photon helicities [10]. The limits on Q_i^2, $|\ln(Q_1^2/Q_2^2)|$ and W_{had} are the same as described above. The differential cross-sections $d\sigma_{ee}/dY$, both for data and MC, and $d\sigma_{\gamma^*\gamma^*}/dY$ are all presented in Table 1. The selection efficiency is calculated using the mean of the results using TWOGAM and PYTHIA. The difference between the results using these two generators is used to calculate the systematic error due to modeling and is in included in the quoted systematic uncertainties. The flux binned over Y is presented as well. The absolute uncertainties on the dL_{TT}/dY calculations are of the order of 0.002×10^{-3}.

Y	$(d\sigma_{ee}/dY)_{data}$ (pb)	$(d\sigma_{ee}/dY)_{MC}$ (pb)	dL_{TT}/dY ($\times 10^3$)	$d\sigma_{\gamma^*\gamma^*}/dY$ (nb)
	no $\ln(Q_1^2/Q_2^2)$ cut		$-1 < \ln(Q_1^2/Q_2^2) < 1$	
(−3)-(−2)	0.02±0.01(stat)±0.01(syst)	0.02±0.01	0.060	0.20±0.11(stat)±0.06(syst)
(−2)-(−1)	0.13±0.04(stat)±0.01(syst)	0.11±0.02	0.114	0.56±0.18(stat)±0.15(syst)
(−1)-0	0.17±0.04(stat)±0.02(syst)	0.26±0.03	0.113	0.89±0.23(stat)±0.21(syst)
0-1	0.42±0.06(stat)±0.08(syst)	0.48±0.01	0.090	2.50±0.49(stat)±0.58(syst)
1-2	0.41±0.04(stat)±0.01(syst)	0.48±0.01	0.082	3.56±0.42(stat)±0.08(syst)
2-3	0.30±0.03(stat)±0.02(syst)	0.32±0.01	0.070	3.00±0.33(stat)±0.19(syst)
3-4	0.25±0.02(stat)±0.01(syst)	0.15±0.01	0.054	2.83±0.32(stat)±0.02(syst)
4-5	0.08±0.01(stat)±0.01(syst)	0.06±0.01	0.034	1.47±0.29(stat)±0.07(syst)
5-6	0.09±0.03(stat)±0.02(syst)	0.02±0.01	0.015	3.51±1.33(stat)±0.60(syst)

Table 1: The measured and expected differential cross-sections $(d\sigma_{ee}/dY)_{data}$ of the reaction $e^+e^- \to e^+e^- + hadrons$, the calculated photon flux L_{TT} including the radiative corrections [7], and the measured cross-section $d\sigma_{\gamma^*\gamma^*}/dY$ of the process $\gamma^*\gamma^* \to hadrons$ are shown as a function of the variable Y.

The measured differential cross-section $d\sigma_{\gamma^*\gamma^*}/dY$ is shown in figure 9. The systematic uncertainties are dominated by the difference between the results obtained with TWOGAM and PYTHIA Monte Carlo generators. The other systematic uncertainties, calculated by varying the selection criteria, the Q^2 domain, etc. represent between 17% and 29% of the statistical uncertainties. The predictions of the QPM and of BFKL calculations, both in LO [12] and NLO [13], are also shown in figure 9. The two curves for the BFKL calculations correspond to the Regge scale parameter s_0, which defines the start of the asymptotic regime, equal to Q^2 or $4Q^2$. The LO calculations are more affected by the uncertainty coming from the choice of the scale parameter than the NLO ones. Note that the BFKL calculations are weighted over a number of Q^2 bins and that therefore the running of α_s is also included. The data lie in any case much lower than the BFKL cross-sections calculated in leading-order. On the other hand, the data are closer to NLO predictions, since the expected growth of the gluon exchange contribution (BFKL) is much weaker and appears mainly for Y values larger than 4. Below this value the cross-section is dominated by the decrease of the QPM contribution. Unfortunately the LEP energy and the present statistics are not sufficient to study in detail the region at large Y, where BFKL is expected to dominate.

5 Conclusions

Double-tagged $\gamma^*\gamma^*$ interactions have been studied with the DELPHI data taken at e^+e^- centre-of-mass energies from 189 GeV to 209 GeV and corresponding to an integrated luminosity of 550 pb^{-1}. For virtualities, Q^2, of both photons between 10 GeV^2 and 200 GeV^2 and final state invariant mass W above 2 GeV/c^2, the cross-section of the process $e^+e^- \to e^+e^- + \mu^+\mu^-$ is measured to be $(1.38\pm0.12(stat) \pm 0.06(syst))$ pb, to be compared with the expectation of (1.36±0.01) pb for the QED calculations including radiative corrections to the photon flux. The cross-section σ_{ee} of the $e^+e^- \to e^+e^- + hadrons$ interactions is measured to be $(2.09 \pm 0.09(stat) \pm 0.19(syst))$ pb with the corrections for detector effects based on the TWOGAM event generator [7]. The differential cross-section $d\sigma_{\gamma^*\gamma^*}/dY$ of the $\gamma^*\gamma^* \to hadrons$ interactions is measured and is compared with the predictions based on LO and NLO BFKL calculations. The leading order calculations clearly disagree with the data while the next-to-leading order predictions are found to be more consistent with the data, although the LEP energy is not sufficient to see a sizable effect due to the BFKL type contribution. The DELPHI data are in agreement with the results of the other LEP experiments [14].

Acknowledgements

We are greatly indebted to our technical collaborators, to the members of the CERN-SL Division for the excellent performance of the LEP collider, and to the funding agencies for their support in building and operating the DELPHI detector.
We acknowledge in particular the support of
Austrian Federal Ministry of Education, Science and Culture, GZ 616.364/2-III/2a/98,
FNRS–FWO, Flanders Institute to encourage scientific and technological research in the industry (IWT), Belgium,
FINEP, CNPq, CAPES, FUJB and FAPERJ, Brazil,
Czech Ministry of Industry and Trade, GA CR 202/99/1362,
Commission of the European Communities (DG XII),
Direction des Sciences de la Matière, CEA, France,
Bundesministerium für Bildung, Wissenschaft, Forschung und Technologie, Germany,
General Secretariat for Research and Technology, Greece,
National Science Foundation (NWO) and Foundation for Research on Matter (FOM), The Netherlands,
Norwegian Research Council,
State Committee for Scientific Research, Poland, SPUB-M/CERN/PO3/DZ296/2000, SPUB-M/CERN/PO3/DZ297/2000, 2P03B 104 19 and 2P03B 69 23(2002-2004)
FCT - Fundação para a Ciência e Tecnologia, Portugal,
Vedecka grantova agentura MS SR, Slovakia, Nr. 95/5195/134,
Ministry of Science and Technology of the Republic of Slovenia,
CICYT, Spain, AEN99-0950 and AEN99-0761,
The Swedish Research Council,
Particle Physics and Astronomy Research Council, UK,
Department of Energy, USA, DE-FG02-01ER41155.
EEC RTN contract HPRN-CT-00292-2002.
We thank the ALEPH Collaboration for the production of the simulated "Cetraro Samples".

References

[1] DELPHI Collab., P. Aarnio *et al.*, Nucl. Instr. and Meth. **A303** (1991) 233;
DELPHI Collab., P. Abreu *et al.*, Nucl. Instr. and Meth. **A378** (1996) 57.

[2] H.G. Dosch, T. Gousset and H.J. Pirner, Phys. Rev. **D57** (1998) 1666.

[3] E.A. Kuraev, L.N. Lipatov and V.S. Fadin, Sov. Phys. JETP **45** (1977) 199;
Ya.Ya. Balitski and L.N. Lipatov, Sov. J. Nucl. Phys. **28** (1978) 822.

[4] DELPHI STIC Collab., S.J. Alvsvaag *et al.*, Nucl. Instr. and Meth. **A425** (1999) 106.

[5] DELPHI Trigger Group, A. Augustinus *et al.*, Nucl. Instr. and Meth. **A515** (2003) 782.

[6] F. Berends, P. Daverveldt and R. Kleiss, Comput. Phys. Commun. **40** (1986) 271, 285 and 309.
h

[7] TWOGAM event generator, T. Alderweireld *et al.*, CERN Report 2000-009, p.219 (2000), edited by G. Passarino, R. Pittau and S. Jadach.

[8] T. Sjöstrand, Comput. Phys. Commun. **82** (1994) 74.

[9] S. Jadach, B.F.L. Ward and Z. Was, Comput. Phys. Commun. **130** (2000) 260.

[10] V.M. Budnev, I.F. Ginzburg, G.V. Meledin and V.G. Serbo, Phys. Rep. **15** (1975) 181.

[11] S.J. Brodsky, F. Hautmann and D.E. Soper, Phys. Rev. **D56** (1997) 6957.

[12] J. Bartels, C. Ewerz and R. Staritzbichler, Phys. Lett. **B492** (2000) 56;
C. Ewerz, private communication.

[13] V.T. Kim, L.N. Lipatov and G.B. Pivovarov, "The next-to-leading BFKL pomeron with optimal renormalization", Proceeding of the International Conference on elastic and diffractive scattering 1999, Protvino, Russia, ed. V.A. Petrov and A.V. Prokudin, World Sci., Singapore (2000) 237, hep-p/9911228;
V. Kim, private communication.

[14] ALEPH Collab., A. Heister *et al.*, CERN-EP/2003-025; hep-ex0305107;
L3 Collab., P. Achard *et al.*, Phys. Lett. **B531** (2002) 39;
OPAL Collab., G. Abbiendi *et al.*, Eur. Phys. J. **C24** (2002) 17.

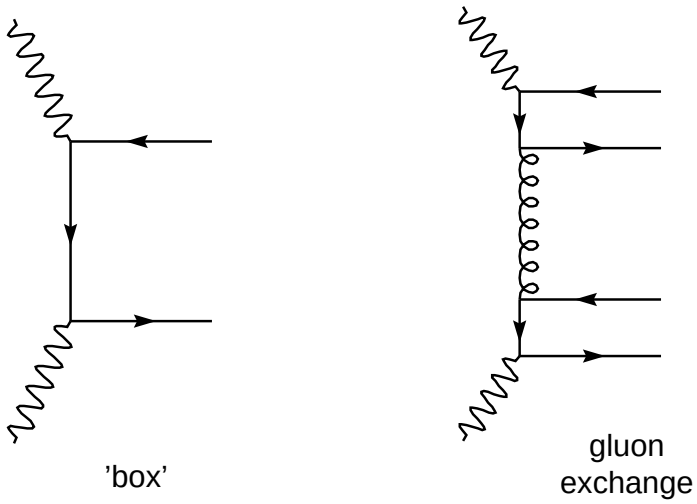

Figure 1: Main diagrams corresponding to the $\gamma^*\gamma^* \to hadrons$ process.

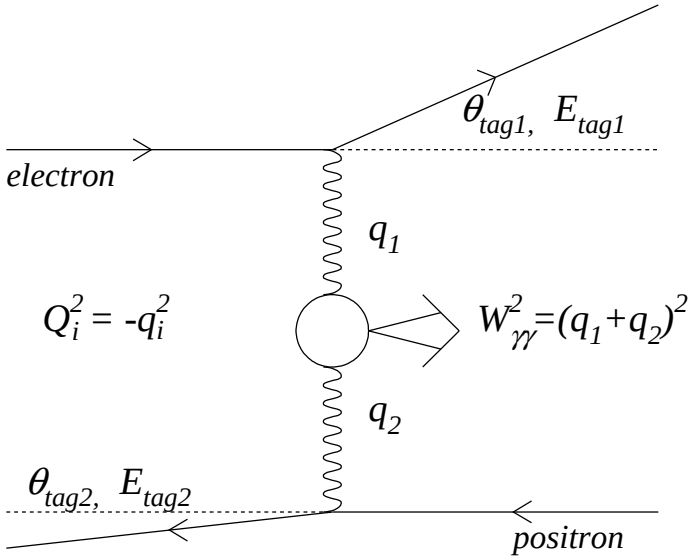

Figure 2: The kinematics of $\gamma^*\gamma^*$ interactions.

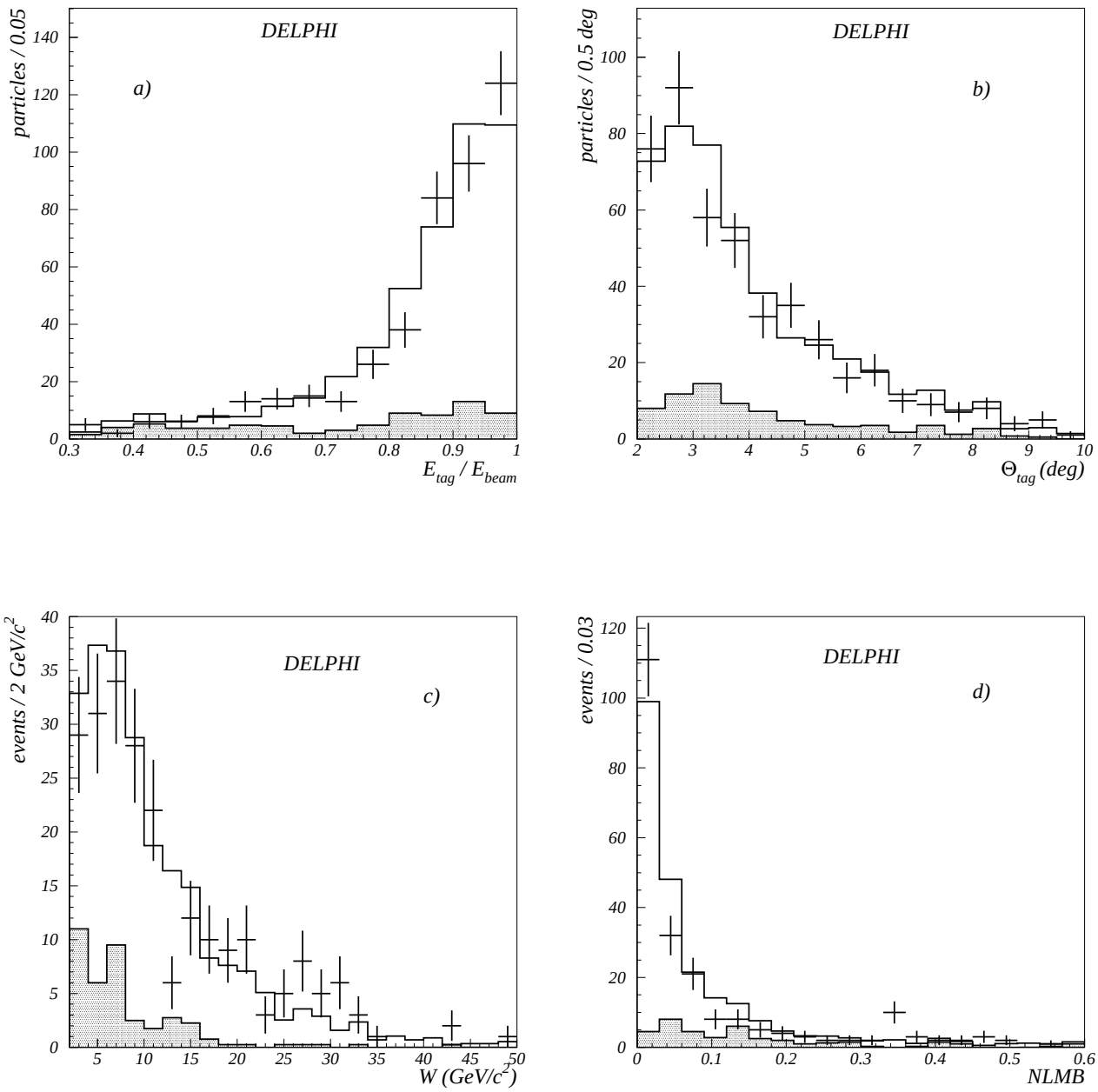

Figure 3: (a) Normalized tagged particle energy E_i/E_{beam}, (b) tagged particle polar angle θ_i (two entries per event for both), (c) invariant mass of the muon pair $W_{\mu\mu}$ and (d) $NLMB$ variable. The data are shown with error bars; the histograms are the sum of the BDKRC simulated events and of the estimated background. The hatched areas represent the background contamination.

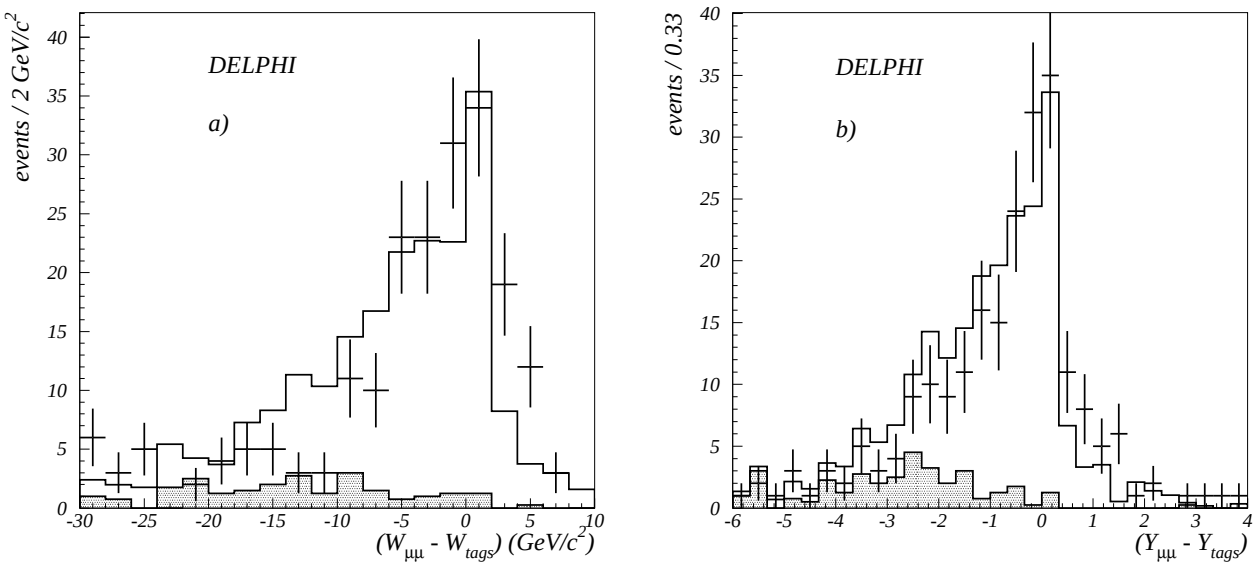

Figure 4: (a) Difference between the invariant mass of the muon pair, $W_{\mu\mu}$, and the invariant mass calculated from the tagged particles. (b) The same for the Y variable. The data are shown with error bars; the dashed histograms are the sum of the BDKRC simulated events and of the estimated background. The hatched areas represent the background contamination.

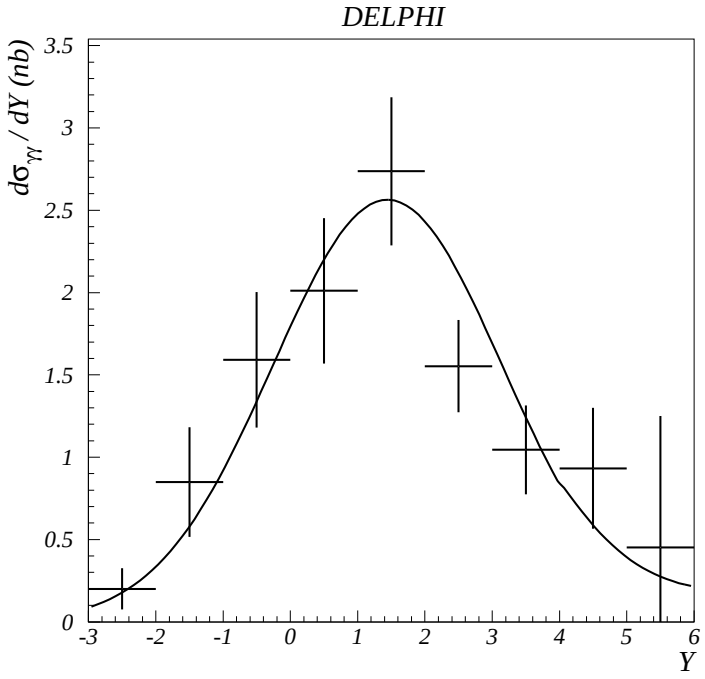

Figure 5: The differential cross-section for the reaction $\gamma^*\gamma^* \to \mu^+\mu^-$. The data are shown with error bars. The solid line shows the QED expectation.

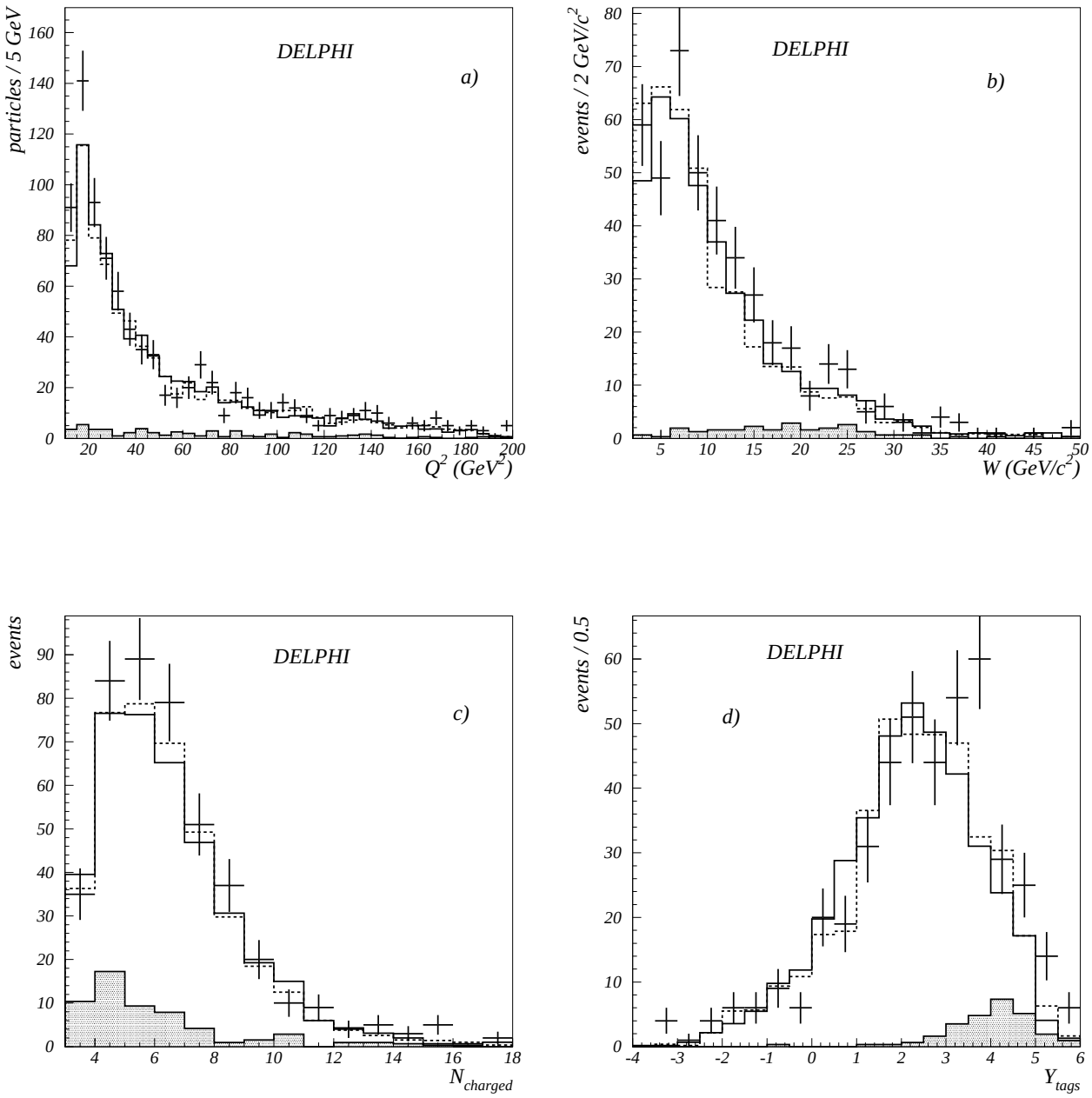

Figure 6: Distributions of Q_i^2 (a), invariant mass W_{had} (b), charged multiplicity $N_{charged}$ (c), and Y calculated from the tagged particles' 4-momenta (d). The data are shown with error bars. The solid and dashed histograms correspond to the sum of $\gamma^*\gamma^*$ simulated events obtained with the PYTHIA and TWOGAM generators, respectively, and include the total background, shown hatched.

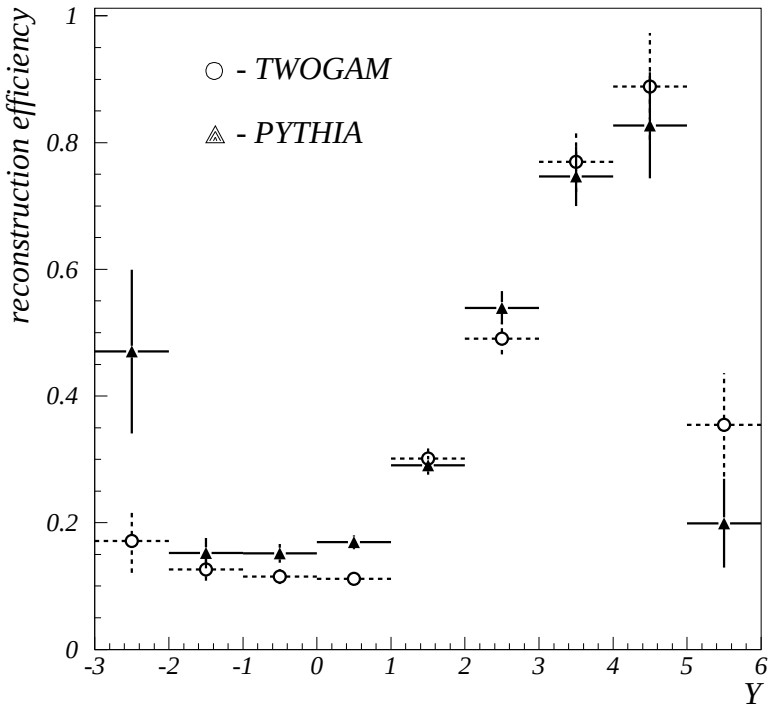

Figure 7: Reconstruction efficiency as a function of Y. The results of the calculations based on TWOGAM and PYTHIA generators are shown.

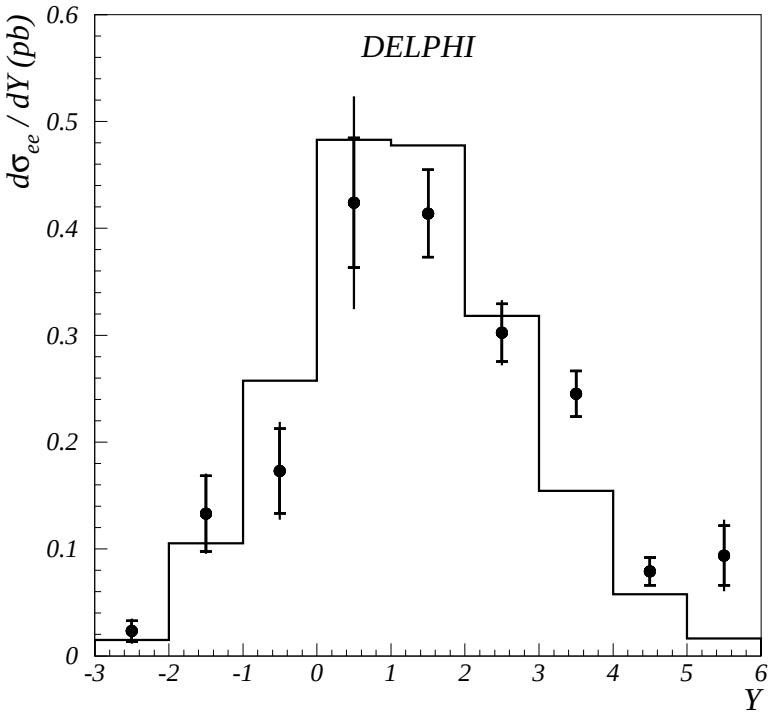

Figure 8: Differential cross-section for the reaction $e^+e^- \to e^+e^- + hadrons$. The dashed histogram corresponds to the average of the TWOGAM and PYTHIA predictions. The data are shown with error bars: the total error bars indicate the sum in quadrature of the statistical (inner error bars) and of the systematic uncertainties.

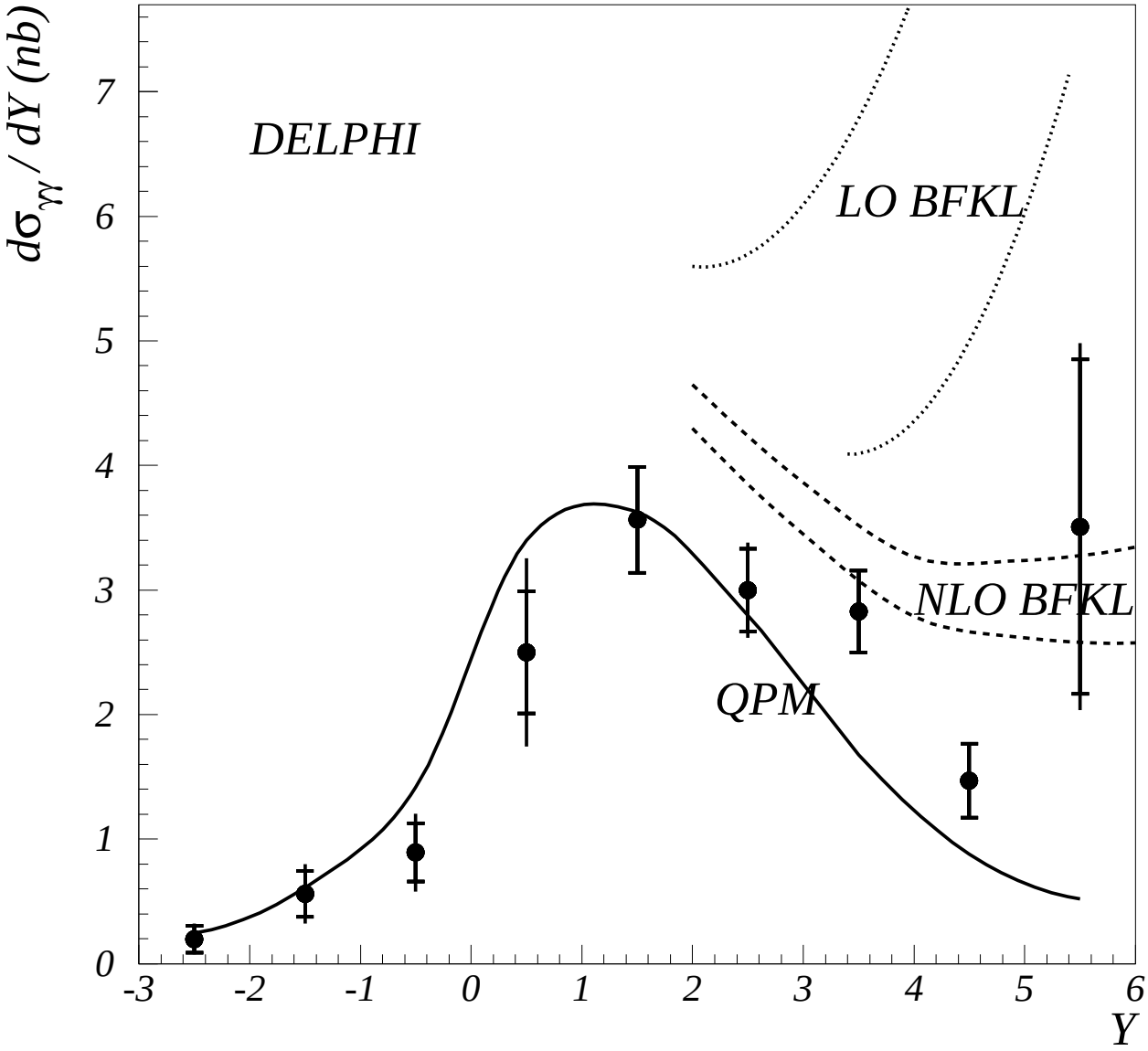

Figure 9: The differential cross-section for the reaction $\gamma^*\gamma^* \to hadrons$. The data are shown with error bars: the total error bars indicate the sum in quadrature of the statistical (inner error bars) and of the systematic uncertainties. The solid curve corresponds to the expectation of the quark-parton model (QPM, quark-box diagram, figure 1). The two dotted lines represent the BFKL calculations in the leading order [12]. The next-to-leading order calculations [13] are shown by the two dashed curves in the middle. The two curves for the BFKL calculations correspond to the Regge scale parameter changing between Q^2 (upper line) and $4Q^2$ (lower one). The QPM contribution is added to both the LO and the NLO BFKL expectations.